Overview of transport and MHD stability study: focusing on the impact of magnetic field topology in the Large Helical Device

Overview of transport and MHD stability study : focusing on the impact of magnetic field topology in the Large Helical Device

K. Ida,[1,2] K. Nagaoka,[1,2] S.Inagaki,[3] H. Kasahara,[1] T. Evans,[4] M. Yoshinuma,[1,2] K. Kamiya,[5] S. Ohdach,[1,2] M. Osakabe,[1] M. Kobayashi,[1,2] S. Sudo,[1,2] K. Itoh,[1] T. Akiyama,[1] M. Emoto,[1] A. Dinklage,[6] X. Du,[2] K. Fujii,[7] M. Goto,[1,2] T. Goto,[1] M. Hasuo,[7] C. Hidalgo,[8] K. Ichiguchi,[1] A. Ishizawa,[1,2] M. Jakubowski,[6] G. Kawamura,[1] D. Kato,[1,2] S. Morita,[1,2] K. Mukai,[1] I. Murakami,[1] S. Murakami,[9] Y. Narushima,[1,2] M. Nunami,[1,2] N. Ohno,[10] N. Pablant,[11] S. Sakakibara,[1,2] T. Seki,[1] T. Shimozuma,[1] M. Shoji,[1] K. Tanaka,[1] T. Tokuzawa,[1] Y. Todo,[1,2] H. Wang,[1] M. Yokoyama,[1,2] H. Yamada,[1,2] Y. Takeiri,[1,2] T. Mutoh,[1,2] S. Imagawa,[1,2] T. Mito,[1,2] Y. Nagayama,[1,2] K.Y. Watanabe,[1] N. Ashikawa,[1,2] H. Chikaraishi,[1,2] A. Ejiri,[12] M. Furukawa,[13] T.Fujita,[10] S. Hamaguchi,[1] H. Igami,[1] M. Isobe,[1,2] S. Masuzaki,[1] T. Morisaki,[1] G. Motojima,[1] K. Nagasaki,[14] H. Nakano,[1] Y. Oya,[15] C. Suzuki,[1] Y. Suzuki,[1,2] R. Sakamoto,[1,2] M. Sakamoto,[16] A. Sanpei,[17] H. Takahashi,[1] H. Tsuchiya,[1] M. Tokitani,[1] Y. Ueda,[18] Y. Yoshimura,[1] S. Yamamoto,[14] K. Nishimura,[1] H. Sugama,[1] T. Yamamoto,[1] H. Idei,[3] A. Isayama,[5] S. Kitajima,[19] S. Masamune,[17] K. Shinohara,[5] P.S. Bawankar,[2] E. Bernard,[1] M. von Berkel,[1] H. Funaba,[1,2] X.L. Huang,[2] T. Ii,[1] T. Ido,[1] K. Ikeda,[1] S. Kamio,[1] R. Kumazawa,[1] T. Kobayashi,[1] C. Moon,[1] S. Muto,[1,2] J. Miyazawa,[1,2] T. Ming,[1] Y. Nakamura,[1,2] S. Nishimura,[1] K. Ogawa,[1] T. Ozaki,[1] T. Oishi,[1,2] M. Ohno,[2] S. Pandya,[2] A. Shimizu,[1] R. Seki,[1] R. Sano,[2] K. Saito,[1] H. Sakaue,[1] Y. Takemura,[1] K. Tsumori,[1,2] N. Tamura,[1] H. Tanaka,[1] K. Toi,[1] B. Wieland,[1] I. Yamada,[1] R. Yasuhara,[1] H. Zhang,[2] O.Kaneko,[1,2] A. Komori,[1,2] and Collaborators*

[1]*National Institute for Fusion Science, Toki, Gifu 509-5292, Japan*
[2]*The Graduate University for Advanced Studies, 322-6 Oroshi, Toki, Gifu 509-5292, Japan*
[3]*Research Institute for Applied Mechanics, Kyushu University, 6-1 Kasuga-kouen, Kasuga, Fukuoka 816-8580, Japan*
[4]*General Atomics, San Diego, CA, USA*
[5]*Japan Atomic Energy Agency, Naka, Ibaraki 311-0193, Japan*
[6]*Max-Planck-Institut für Plasmaphysik, Wendelsteinstr. 1, 17489 Greifswald, Germany*
[7]*Department of Mechanical Engineering and Science, Graduate School of Engineering, Kyoto University, Kyoto 606-8501, Japan*
[8]*Laboratorio Nacional de Fusion, Asociacion EURATOM-CIEMAT, 28040 Madrid, Spain*
[9]*Department of Nuclear Engineering, Kyoto University, Kyoto 606-8501, Japan*
[10]*Department of Energy Engineering and Science, Nagoya University, Furo-cho, Chikusa, Nagoya 464-8603, Japan*
[11]*Princeton Plasma Physics Laboratory, PO Box 45, Princeton, NJ 08543-0451, USA*
[12]*Graduate School of Frontier Sciences, The University of Tokyo, 5-1-5 Kashiwanoha, Kashiwa-shi, Chiba-ken 277-8561, Japan*
[13]*Department of Applied Mathematics and Physics Faculty of Engineering, Tottori University, 4-101 Koyama-Minami, Tottori 680-8552 Japan*
[14]*Institute of Advanced Energy, Kyoto University, Kyoto 611-0011, Japan*
[15]*Radioscience Research Laboratory, Faculty of Science, Shizuoka University, 836 Oya, Suruga-ku, Shizuoka 422-8529, Japan*
[16]*Plasma Research Center, University of Tsukuba, 1-1-1 Tennodai, Tsukuba, Ibaraki 305-8577, Japan*
[17]*Kyoto Institute of Technology, Matsugasaki, Sakyo-ku, Kyoto 606-8585, Japan*
[18]*Graduate School of Engineering, Osaka University, 1-1 Yamadaoka, Suita, Osaka 565-0871, Japan*
[19]*Department of Quantum Science and Energy Engineering, Tohoku University, Sendai 980-8579, Japan*

(Dated: January 30, 2015)

The progress of physics understanding and concurrent parameter extension since the last IAEA-FEC 2012[1] in the Large Helical Device is overviewed. High ion and electron temperature plasma ($T_i(0) \sim T_e(0) \sim 6$ keV) with simultaneous ion and electron internal transport barrier (ITB) is obtained by controlling recycling and heating deposition. Associated with the formation of a transport barrier, a sign flip of the non-diffusive term of impurity/momentum transport (residual stress and convection flow) is observed. The impact of the topology of 3-D magnetic fields (stochastic magnetic fields and magnetic islands) on heat momentum and particle/impurity transport and MHD stability is also discussed. In the steady state operation, a 48 min discharge with a line-averaged electron density of $1 \times 10^{19}\mathrm{m}^{-3}$ and with high electron and ion temperatures ($T_i(0) \sim T_e(0) \sim 2$keV) resulting in 3.36 GJ of input energy is achieved.

PACS numbers: 52.55.Hc, 52.55.Fa, 52.50.Sw, 52.50.Gj

I. INTRODUCTION

Simultaneous achievement of high electron (T_e) and ion temperature (T_i) is one of the most important issues in nuclear fusion research. On the other hand, an anoma-

lous ion thermal transport is sensitive to T_e/T_i ratio[2], thus the formation of electron and ion internal transport barrier (ITB) with optimizing T_e/T_i ratio is necessary for the simultaneous achievement of high T_i and high T_e. In a helical system, because the safety factor (q) profile is mainly determined by external coils, the effect of T_e/T_i ratio on the thermal transport can be investigated separately from q profiles, which usually has strong influence in tokamaks. The other advantage of helical plasmas is that the steady-state operation can be realized without a delicate plasma current control. Therefore, the key issue for the achievement of long pulse is the control of plasma wall interaction, which will be also important in future tokamak devices such as ITER. By taking advantage of the easy realization of the steady-state plasma, the detailed transport analysis especially in response to the perturbation, such as modulation ECH or pellet injection, has been carried out by using conditional averaging technique.

The impact of 3-D magnetic fields on transport and MHD stability is also intensively studied in the Large Helical Device (LHD) where the intrinsic 3-D magnetic fields (stochastic magnetic fields and magnetic islands) always exist in the plasma and are well controlled. The transport inside a magnetic island has been an interesting topic in toroidal plasma. The LHD provides a good platform for this study because there is no risk for disruption even in the plasma with a locked big magnetic island, where the detailed study of transport can be undertaken. The impurity control by 3-D magnetic fields is one of the important topics in LHD, because these results give insight regarding impurity control in tokamaks under the condition with RMP in tokamaks. In this overview, the recent achievement of plasma parameters and the new understanding of physics on turbulence transport and the impact of magnetic topology on transport and MHD are discussed.

II. EXTENSION OF OPERATION REGIME IN LHD

In the LHD, the ion-ITB and electron-ITB have been obtained separately with different densities and heating methods (NBI or ECH)[3]. Recently, the plasma with high ion and electron temperature ($T_i(0) \sim T_e(0) \sim 6$ keV) has been obtained by the combination of 1) a reduction of wall recycling and neutrals by Helium ICRF discharges and 2) optimization of carbon pellet injection[4] and on-axis ECH[5, 6]. In LHD, neutral hydrogen atom density, temperature, and pressure distributions from edge to core regions are evaluated from the high dynamic-range Balmer-α line profile analyzed with a diffusion equation of hydrogen atoms [7, 8].

The temperature regime obtained is significantly extended, as seen in Fig. 1. The electron density and total heating power in the plasmas plotted in Fig. 1 is $0.4 - 2.0 \times 10^{19}\mathrm{m}^{-3}$ and 22 - 31 MW (NBI 20 - 27 MW and ECH 2 -4 MW). The stochastic magnetic field in the plasma core which causes flattening of the temperature and the plasma flow can be eliminated by the control of the magnetic shear by NBCD and ECCD. A high central ion temperature ($T_i(0) \sim 8$ keV) discharge is achieved by avoiding the core temperature flattening due to the stochastization frequently observed in the plasma with an ion-ITB by controlling the magnetic shear at the rational surface. Simultaneous formation of an ion ITB and an electron ITB has been successfully achieved by controlling the temperature profiles using ECRH. The width of the ion ITB is larger than that of the electron ITB. The temperature gradients evaluated as the ratio of major radius to the temperature scale length, R/L_T, both for ions and for electrons were over 10 inside the ITB, and both T_i and T_e reached 6 keV. The T_i gradient at the ion ITB is found to be decreased when T_e/T_i value exceeds unity due to the increase of the anomalous transport. As a result of the dependence, the combination of a wide ion ITB and a narrow electron ITB with $T_i > T_e$ is realized. This study demonstrated that profile control is a key to combining the ion ITB and the electron ITB and to have a potential to improve the performance of toroidal plasma plasmas.

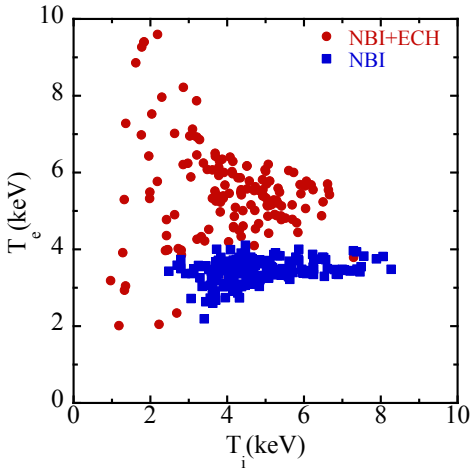

FIG. 1: Operation regime of central electron and ion temperatures for the discharges with NBI and NBI+ECH in LHD.

High ion temperature plasma with carbon pellet injection of LHD is investigated by the integrated heat transport simulation. NBI heating deposition of time evolving plasma is evaluated by GNET- TD[9] and the heat transport of multi-ion species plasma (e, H, He, C) is studied by TASK3D[11, 12]. The integrated heat transport simulation code shows that the reduction of the turbulent transport, by more than a factor of three as compared with the L-mode case, is the most significant contribution to achieving the high ion temperature.

In steady-state operation, plasma parameters have

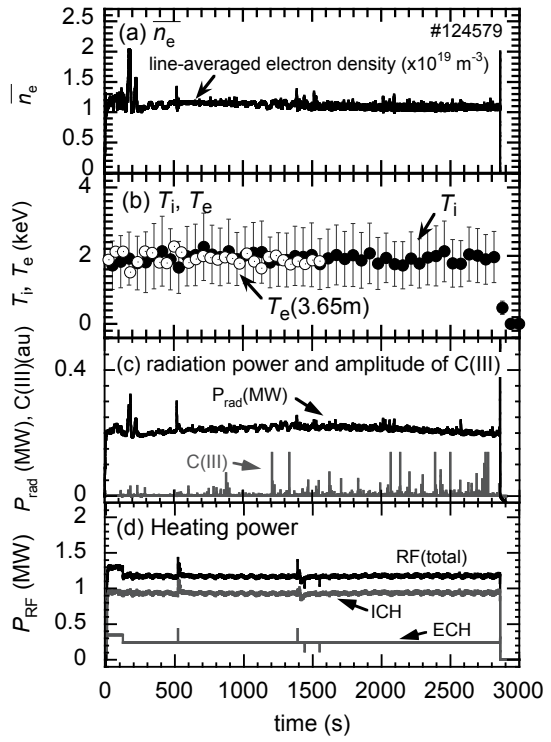

FIG. 2: Ultra long-pulse plasma sustained by RF heating for hydrogen minority helium plasma. Typical time evolutions are as follows: (a) line-averaged electron density (ne), (b) ion (Ti) and central electron temperature (Te), (c) total radiation power and line intensity of carbon spectrum, and (d) RF heating powers of ICH and ECH (from Fig.2 in [14]).

been extended at line-averaged electron density measured with the interferometer[13] of $1\times10^{19}\mathrm{m}^{-3}$ with high electron and ion temperature ($T_i(0) \sim T_e(0) \sim$ 2keV) and plasma duration time of 48 min with 3.36 GJ of input energy by minimizing the dust impurity from the divertor plate by real time divertor leg scanning. A new type of temperature fluctuation with a low frequency of nf (f = 0.55 kHz, n = 1,2,3,4) is observed for the first time by accumulating the fluctuation spectra measured in a long pulse discharge[14]. Figure 2 shows an ultra-long-pulse plasma discharge of a helium plasma with $n_e \sim 1\times10^{19}\mathrm{m}^{-3}$, $T_e \sim T_i \sim$ 2keV, $P_{RF} \sim$ 1.2 MW ($P_{ICH} \sim$ 0.9 MW, $P_{ECH} \sim$ 0.3 MW), and $\tau_d \sim$ 2,859 sec. The newly achieved heating energy of 3.36 GJ is a world record in toroidal plasmas and it doubles the previous record, 1.6 GJ, obtained with $P_{RF} \sim$ 0.5MW and $n_e \sim 0.4\times10^{19}\mathrm{m}^{-3}$ in LHD[15].

Three types of ICRF antennas were installed at different toroidal sections in order to compare the heating efficiency, loading resistance and the enhancement of impurity influx causes by the ICRF heating. They are 1) the field aligned toroidal array antenna, 2) the field-aligned impedance-transforming poloidal array antenna (FAIT antenna), and 3) the conventional poloidal array antenna with and without Faraday Shield (FS). The field aligned toroidal array antennas have higher heating efficiency and lower impurity influx than conventional antenna without field alignment and the highest heating efficiency is obtained with the field aligned toroidal array antenna. In contract, poloidal array antennas have higher loading resistance and better plasma coupling than toroidal array antenna. The field-aligned impedance-transforming poloidal array antenna (FAIT antenna) has the highest loading resistance and better heating efficiency. The effects of Faraday Shield (FS) on loading resistance and heating efficiency are investigated using the conventional poloidal array antenna. Although the antenna without FS has better coupling (higher loading resistance) than the antenna without FS, the heating efficiency and impurity influx do not clearly depend on with/without FS. In order to maintain the steady-state high-performance plasma duration using these ICRF antennas, real-time feedback control for impedance matching, antenna phasing and heating power boosting for unexpected impurity influx were also developed. Steady-state high power heating with MW-class was successfully achieved using ICRF and ECH[16].

Wall pumping was gradually reduced during the long-pulse discharge with $\tau_d >$ 1000 sec. The gas-fueling by a proportional-integral-derivative (PID) control was adopted to maintain a constant level of the plasma density, as shown in Fig. 2(a). Radiation power (P_{rad}) was less than approximately 17% of P_{RF}, where the carbon and iron impurity[17, 18] accumulation was negligible in the discharge. The frequency of the spikes of the carbon III line intensity for the carbon spectrum began to increase after 600 sec. At that time, the divertor temperature was almost saturated at 460^o C, while the value changed between 453 and 470^o C by magnetic axis sweeping to reduce the local heat load on divertor plates. This experiment demonstrates the importance of the control of divertor temperature in the steady-state operation, because the discharge is terminated by the radiation collapse triggered by the bursty impurity flux from the divertor plate in LHD. The additional heating by ECH could be useful tool to avoid the radiation collapse, because the impurity can be exhausted in the electron root plasma with positive electric field as demonstrated in the short pulse discharges with Neon injection[19].

The mixed-material layer in the divertor plate is easily separated from the thin iron layer due to the mechanical and heat stress. This mixed-material is one of the possible sources for the carbon impurity content after 300 sec, which is caused by erosion on the divertor and short-distance transport[20]. Many incandescent dusts have been observed in this long pulse discharges with tangentially viewing fast framing cameras. The dusts induce frequent spikes of emission of iron and carbon ions measured with a spectrometer. A stereoscopic observation of the three-dimensional trajectories of the dusts in plasmas with higher heating power shows that the dusts exist in the plasma periphery and do not penetrate into the main plasma, while penetration of dust particles were observed

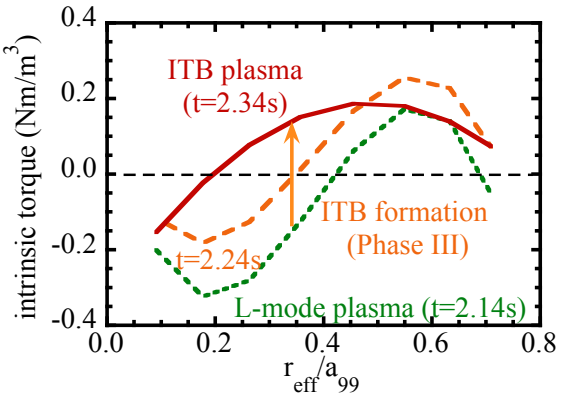

FIG. 3: Radial profiles of intrinsic torque during the formation of ion-ITB (from Fig.6(b) in [22]). Shot numbers are 90493 and 90982.

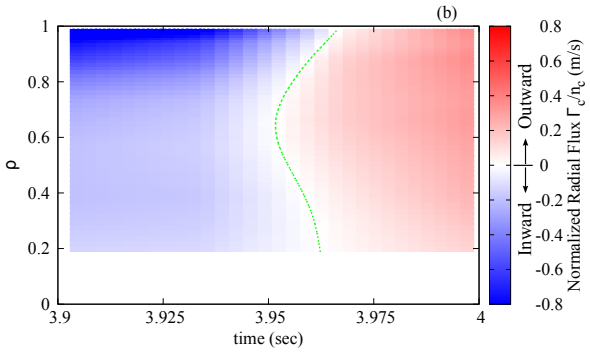

FIG. 4: Spatiotemporal dynamics of radial flux of carbon impurity. The reversal of normalized radial flux from inward to outward is observed. The location for $\Gamma_c = 0$ is indicated with dashed line. Shot number is 101329.

in plasmas with lower heating power[21].

III. TRANSPORT

As seen in Fig. 3, the intrinsic torque due to the residual stress switches the sign from the counter- to the co-direction and results in a large toroidal flow in the co-direction after the formation of the ion-ITB[22]. The ion-ITB discharge is obtained by lowering the T_e/T_i ratio of the target plasma with high power heating[2]. Before the ITB formation, the intrinsic torque is in the counter-direction in the core ($r_{\rm eff}/a_{99} < 0.4$), while it is in the co-direction in the outer region ($r_{\rm eff}/a_{99} > 0.4$). Here $r_{\rm eff}$ and a_{99} are effective minor radius and minor radius which contains 99% of kinetic energy given by mapping process[23]. The intrinsic torques in the core region change sign from the counter-direction to the co-direction after the formation of the ITB, which clearly shows the strong coupling between the heat transport and the momentum transport. The intrinsic torque in the L-mode region is in the counter-direction, while it reverses to the co-direction inside the ITB. The reversal of intrinsic torque from counter-direction to co-direction is observed to be associated with the formation of ion ITB. In the plasma with ion-ITB, the gyrokinetic Vlasov flux-tube code GKV-X[24] predicts that the ITG mode is unstable and the TEM is stabilized due to the increase of the ion temperature gradient and the flattening of the electron density profile[25, 26]. This result is in contrast to the reversal of rotation from co-direction to counter-direction associated with the transition from the TEM to the ITG mode during the density scan[27].

In the impurity transport, the radial convective velocity of the carbon impurity (Vc) also changes sign from inward to outward, and this reversal of radial flux causes the extremely hollow impurity profile (called impurity hole). The radial flux is inward before the ion temperature gradient reaches a critical value of 3.0 keV/m and then the reverse of normalized radial flux to outward is observed at t = 3.96 s within a very short time of 30 ms where the ion temperature gradient changes by 10%. The outward radial flux is kept during the discharge even though the ion temperature gradient decreases below the critical value. Figure 4 shows the normalized radial flux of carbon impurity in time and space during the formation of the impurity hole[28]. The radial flux of carbon impurity is derived from the time evolution of fully ionized carbon density measured with charge exchange spectroscopy. The reversal of radial flux starts at $r_{\rm eff}/a_{99} = 0.65$ where the ITB also starts and propagates both inward and outward in the time scale of 15 ms. It should be noted that this time scale is much shorter than the time scale of change in the mean plasma parameter, which indicated that the radial impurity flux is not determined by the mean plasma parameters but is strongly influenced by the turbulence state. Comprehensive electrostatic gyrokinetic linear stability calculations for ion-scale microinstabilities in an LHD plasma with an ion-internal transport barrier (ITB) and carbon impurity hole are used to make quasilinear estimates of particle flux to explore whether microturbulence can explain the observed outward carbon fluxes. As the carbon density gradient is scanned between the measured value and zero, the quasilinear carbon flux is invariably inward when the carbon density profile is hollow, thus turbulent transport due to the instabilities considered here does not explain the observed outward flux of impurities in impurity hole plasmas[29]. There is no impurity hole observed in the long pulse operation. This is because the temperature gradient in the L-mode long pulse is lower than the critical temperature gradient for the formation of impurity hole[30].

Modulated electron cyclotron heating (MECH) has been recognized to be a useful tool to identify the topology of the magnetic field (stochastic field, magnetic island, nested fine flux surfaces) and characteristics of turbulent transport (core-edge transport coupling, radial

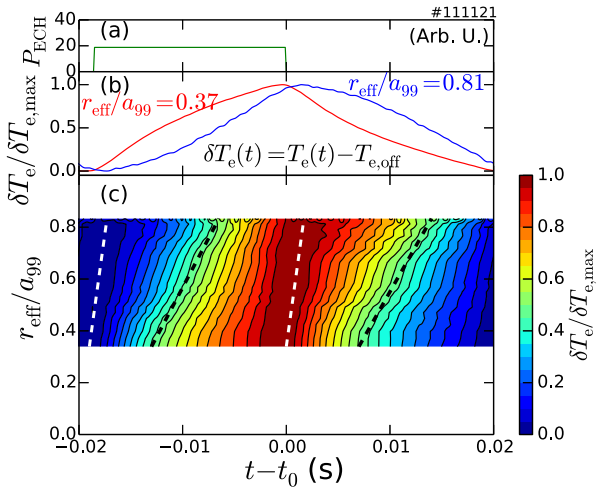

FIG. 5: Time evolution of (a) ECH power, (b) the normalized temperature perturbations at $r_{\rm eff}/a_{99} = 0.37$ and 0.81 and (c) spatiotemporal evolution of δT_e (from Fig.1 in [33]).

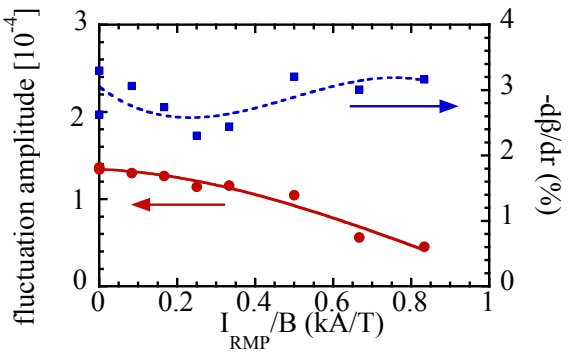

FIG. 6: Magnetic fluctuation level of $m/n = 2/3$ mode and pressure gradient as a function of RMP coil current. The fluctuation decreases as the perturbation field is increased although the pressure gradient is unchanged.

propagation of response)[31]. The location and size of the magnetic island are investigated by MECH. MECH is also applied to investigate the non-local characteristics of heat transport[32]. The radial propagation of the temperature response (T_e rise and drop) due to the on/off of the ECH is found to be much faster than the propagation of the modulation phase by a factor of 5 and the heat pulse intensity with higher harmonics is found to have a propagation length larger than that predicted by the diffusive model[33]. These observations suggest that there is a transport mechanism besides diffusion (e.g., non-locality of transport[34]) in the heat transport.

Figure 5 shows the conditional-averaged periodic modulation of T_e. There are two distinct time scales. The first is the very short time scale. The change of time derivative of T_e at the time of switch-off/on of ECH power propagates in radius very rapidly (white dashed lines), approximately the radial propagation velocity of change in the long-range modes[35]. The second is the much longer time scale. The propagation of Te perturbation follows the slow propagation (a contour line of $\delta T_e(r_{\rm eff}, t)/\delta T_{e,\max}(r_{\rm eff}) = 0.5$ is chosen as a reference and shown as black dashed lines) of the order of the global energy confinement time scale. Faster radial propagation of the higher harmonic component of heat pulse than the fundamental component is also observed in the MECH experiment in TJ-II[36]. These phenomena show that the non-linearity of transport appears in the radial propagation sped of heat pulse, because the higher harmonic component, which contains fast change of temperature gradient, propagates faster, while the gradual change of temperature gradient in the fundamental mode propagates in the so-called transport time scale.

IV. MHD STABILITY

Effects of low-n MHD instabilities on plasma performance have been assessed in the regime where an achieved beta value is regulated by instabilities. The unstable regime of an ideal interchange mode is characterized by enhanced magnetic hill and reduced magnetic shear. Experiments have clarified that (i) low-n modes are significantly destabilized in the ideal-unstable configurations and lead to degradation of central beta by at most 60%, and (ii) the degree of their damages strongly depends on the mode rotation velocity[38–40]. Turbulent transport in finite-beta LHD plasmas is investigated by means of electromagnetic gyrokinetic simulations[41].

In the LHD, the magnetic field near the plasma periphery is a stochastic and partially open field lines. Therefore it is an interesting issue how the stochastization of the magnetic field affects the MHD instability driven by a pressure gradient. Apart from the stochastization in the plasma core, the stochastization of the magnetic field is weak (effective thermal diffusivity due to stochastization is comparable to that due to turbulence) enough to sustain a finite pressure gradient. This is an interesting topic because the stochastization of the magnetic field is also a key issue in the resonant magnetic perturbation (RMP) experiment for edge localized mode (ELM) suppression. When the stochastization of the magnetic field is enhanced by the RMP, the pressure driven mode is suppressed even without a change in the pressure gradient itself as seen in Fig. 6. Amplitude of $m/n = 2/3$ and 2/4 modes are reduced by the RMP field when the normalized RMP coil current I_{RMP}/B exceeds 0.7. With the increase of the RMP field, increase of the spectral width Δf (i.e., decrease of the auto correlation function) of the mode is observed[42].

In the LHD, a low mode (n/m=1/1) magnetic island exists near the plasma periphery and the width of the

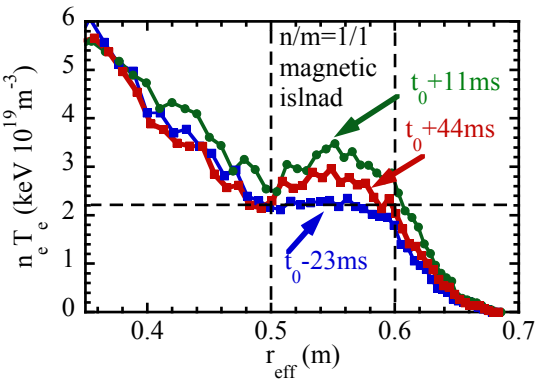

FIG. 7: Pressure profiles in the plasma with an n/m=1/1 magnetic island. A peaked pressure profile is observed inside the magnetic island.

magnetic island can be controlled by the RMP. It has been observed that thresholds of the amplitude of RMP for the healing/growth transition of the magnetic island depend upon magnetic axis position R_{ax}. The RMP threshold for growth of island increases as the magnetic axis position R_{ax} increases[43]. The interaction between pressure driven modes and magnetic islands induced by a resonant magnetic perturbation (RMP) in LHD configuration is analyzed by means of three-dimensional simulations. The deformation of the equilibrium pressure profile changes the structure of the unstable mode from the interchange type to the ballooning type[44].

The n = 1 RMP field leads to rather drastic change in the flux averaged particle transport, that is, enhancement of effective diffusion coefficient[45, 46]. However, the detailed study of particle transport in the O-point and X-point of the magnetic island has not been carried out, in spite of the importance especially in the plasma with RMP. By injecting hydrogen pellets into the O-point of the magnetic island, a significant peaked pressure profile inside the magnetic island is produced for a relatively long time as seen in Fig. 7, which is similar to the phenomena of a snake in a tokamak[47]. The peaking of the pressure, not the density alone, indicates the improvement of transport, because the pressure profiles should be unchanged immediately after the ablation of the pellet in the adiabatic process. This peaked pressure profile can sustain for the long time of > 50 ms, which suggests the reduction of transport inside the magnetic island and consistent with the slow cold pulse propagation inside the magnetic island in LHD[48]. The significant reduction of transport inside the magnetic island is also observed in JT-60U after the back-transition from H-mode to L-mode phase[49].

The impact of the stochastization on the $E \times B$ flow is different (opposite effect) inside and outside of the

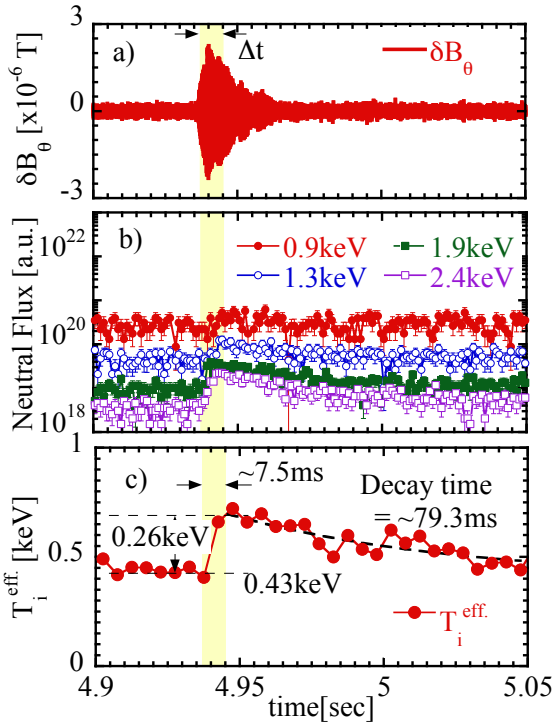

FIG. 8: Typical waveforms of (a)magnetic-fluctuation (Mirnov-coil), (b) neutral flux, and (c) effective ion temperature evaluated from the neutral particle spectra during an EGAM activity (from Fig.1 in [54]).

last closed flux surface (LCFS). Inside the LCFS, the stochastization causes the damping of flows[50]. Outside the LCFS, the electrons are lost along the open field lines, leaving the ions behind and large positive E_r is produced[51]. The location at which the spatial derivative in the E_r structure (∇E_r) has a local maximum value move outwards from the vacuum last closed flux surface location as the volume-averaged plasma beta increases. This fact suggests that the magnetic topology, whether the magnetic field lines are open or closed can be distinguished by the radial structure of E_r and the measurement of E_r would be a useful tool to identify the topology near the plasma periphery when the RMP is applied in tokamak plasmas.

V. ENERGETIC PARTICLES

A new type of MHD instability driven by energetic particles, the helical-ripple trapped energetic ions driven resistive Interchange mode (EIC), has been observed in the ion-ITB plasma in LHD[52]. This mode is characterized by the large change in plasma potential measured by the Heavy Ion Beam Probe system (HIBP) and the increase of neutral flux with energy of 34keV measured with a Compact Neutral Particle Analyzer system (CNPA) syn-

chronizing with each EIC. These observations suggest the enhanced radial transport of energetic ions and redistribution of ions in the velocity space by this mode.

LHD is a good device for this study because it has a high energy neutral beam ($E \sim 180$ keV/amu) and the plasma with a very low density ($n_e \sim \times 10^{18}$ m^{-3}) can be realized. The energetic-particle driven geodesic acoustic mode (EGAM[53]) was observed. An increase of the effective ion temperature is observed during EGAM activity, which implies a possible heating mechanism of the GAM channeling in the slowing down process of energetic particles[54]. Figure 8 shows typical waveforms of (a)magnetic-fluctuation (Mirnov-coil), neutral flux, and effective ion temperature evaluated from the neutral particle spectra during an EGAM activity. This is the first experimental result indicating the increases of ion temperatures with EGAM excitation.

The time scale of the increase of temperature is only 7.5ms. This short time scale of temperature increase suggests that the increase of temperature is due to the additional heating or re-distribution in velocity space of ions and not due to the modification of the transport, because if the improvement of transport occurs, the temperature should increase slowly due to the increase of energy confinement time.

In this experiment, the tangential high energy NB was injected to a very low density plasma of $\sim 5\times10^{17}$m^{-3} for 1 sec. The ion temperature increase with EGAM activity was observed during the ECH superposed phase to the plasma. The typical pulse duration of ECH was 300 ms and the electron temperature was sustained by ECH in the experiment.

VI. EDGE PLASMAS

The 3D effects are elucidated as a consequence of the competition between parallel and perpendicular transport in flux tubes such as open field lines connected to the divertor plates or in magnetic islands[55]. The competition process affects energy, particle, and momentum transport in the divertor/SOL region, which has strong impact on the most important divertor functions, such as density regime, impurity screening, and detachment stability. In LHD, a Ne seeding experiment was conducted, and the enhanced radiation and reduction of the divertor heat flux were confirmed[56].

It has been found that the application of RMP with m/n=1/1, which creates the resonant magnetic island structure in the stochastic region, has a stabilizing effect on the detachment [57]. Without RMP, otherwise, the discharge goes to radiation collapse. The divertor probe array measurements show that the particle flux profile has n=1 mode structure in the toroidal direction during detachment [58]. The 3D numerical simulation with EMC3-EIRENE shows that with RMP application the intense radiation is formed along the trajectory of the X-point of m/n=1/1 island, while without RMP the radiation is localized at the inboard side throughout the torus.

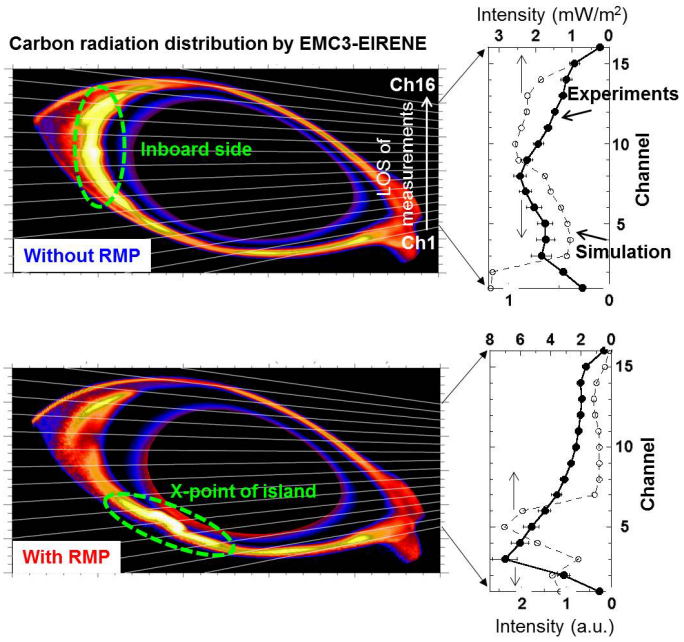

FIG. 9: Comparison of radiation distribution between experiments and simulation (from Fig. 8 and Fig. 9 in [57]).

These experiment and simulation results demonstrate that the advantage of the RMP is a stabilization of detached plasma. By using the RMP, the intense radiation can be localized at the X-point rather than the inboard side and the radiation instability of the detached plasma, where the divertor heat flux is significantly reduced, can be stabilized and hence the radiation collapse can be also avoided.

The radiation distribution measurements with both AXUVD as well as imaging bolometer show the signature of the intense X-point radiation, confirming, at least qualitatively, agreement with the code prediction for modification of 3D radiation structure [59–61], as shown in Fig. 9. In the detached plasma, a broadening of the divertor flux and positive spikes of ion saturation currents, as well as the reduction of the divertor flux at the strike point, were clearly confirmed on the divertor plate[62]. In the simulation, it is clear that the screening effect of parallel flow in the case of high-density discharges prevents accumulation of impurities in the ergodic region and keeps the amount of impurities on the same level as the open configuration[63].

Impurity shielding is also an important issue, because the influx of metal and Carbon impurity from the wall causes the significant degradation of fusion plasma performance. Therefore, study of the shielding effect is important as well as the modeling of sputtering. The stochastic magnetic field and magnetic island have been recognized to contribute to the reduction of impurity in-

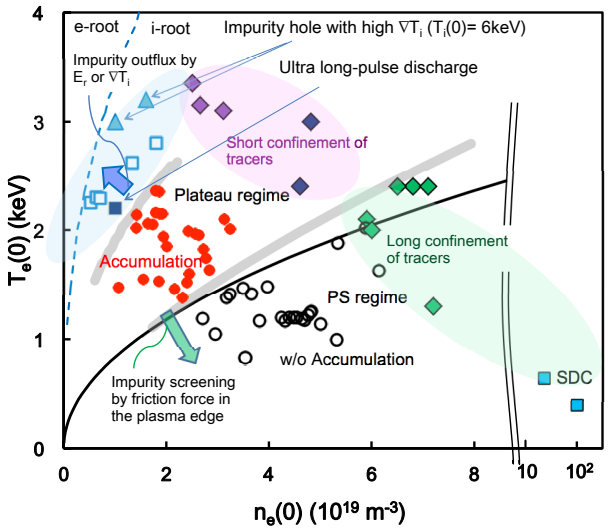

FIG. 10: $n_e(0) - T_e(0)$ diagram showing the property of the impurity transport (Fig.7 in [64]). The data in the ultra long-pulse discharge is plotted with closed square.

flux (impurity shielding). There are two mechanisms to reduce impurity content: one is the outward convection of impurities in the core at low collisionality and the other is shielding effect due to stochastization near the edge at high collisionality. These impurity shielding effects are significant advantages for steady-state operation in the LHD.

Figure 10 shows the summary of the properties of the impurity transport on the $n_e(0) - T_e(0)$ diagram[64]. Although detailed analysis should be done using the local parameters, such a diagram is still useful to see the general trend of the impurity transport. The solid line indicates the line discriminating the collisionality between the PS and plateau regimes. The blue dotted line indicates the line discriminating the conditions between the electron-root (positive radial electric field) and the ion-root (negative radial electric field). SDC means the super dense core plasma[65], where the central electron density reaches $n_e = 1 \times 10^{21}$ m^{-3}. In this SDC plasmas, TESPEL[66] also shows the long tracer confinement. There is a parameter space in n_e and T_e where the impurity accumulation takes place. This parameter space is relatively narrow and most of the discharges in the LHD have no impurity accumulation. In the long pulse operation, although there is no impurity accumulation (gradual increase of radiation), the burst of the large impurity influx from divertor plate causes a sudden increase of radiation and terminates the discharge.

As discussed above, in the high performance plasma such as ion-ITB plasma, the impurity tends to be exhausted. Impurity accumulation on ITB scenarios, which is sometimes observed in tokamaks, will not be the problem in helical plasma. The atomic model for tungsten impurity transport has been developed and applied to analyze spectra observed in LHD. It was found that the extreme ultraviolet lines of W^{24+} to W^{33+} ions were very sensitive to the change of electron temperature and useful to examine tungsten behavior in plasma for future transport study in LHD[67].

VII. SUMMARY

There is significant progress in physics understanding and concurrent parameter extension in the Large Helical Device. In the parameter extension, high ion and electron temperature plasma ($T_i(0) \sim T_e(0) \sim 6$ keV) with simultaneous ion and electron internal transport barrier (ITB) is obtained by controlling recycling and heating. In the steady state operation, a 48 min discharge with a line-averaged electron density of 1×10^{19}m^{-3} and with high electron and ion temperatures ($T_i(0) \sim T_e(0) \sim 2$keV) resulting in 3.36 GJ of input energy is achieved.

The non-diffusive terms of the momentum transport[10] and impurity particle transport has been studied in the ion-ITB plasma. The experimental results show the flip of intrinsic torque and convection of impurity. The time scale of the flip is much shorter than the time scale of the change in mean plasma parameters, which imply the sign of non-diffusive term is directly affected by the turbulence state.

The modulation electron cyclotron heating (MECH) has been applied in order to study the transport especially focusing upon the dynamic response to the perturbation. The transport analysis of the dynamic response for the heat pulse by MECH shows the non-linear and non-diffusive characteristics of transport. The high frequency component of the perturbation propagates much faster than the fundamental component of the modulation. The toroidal rotation at the LCFS, which has been considered to be zero, is found to be affected by the electron temperature gradient near the LCFS. This fact suggests the change in residual stress associated with the modulation of the electron temperature gradient.

The impacts of magnetic topology, especially the magnetic island and stochastic magnetic field on the MHD and transport, have been studied. A significant reduction of magnetic perturbation without the change in pressure gradients is observed when the magnitude of the resonance magnetic perturbation (RMP) field is increased. This result shows the direct effect of magnetic topology on MHD instability, which offers a hint for the mechanism of ELM suppression by RMP in tokamaks.

The peaked pressure is observed inside the magnetic island after the pellet injection to the O-point of the magnetic island, which shows the reduction of transport inside the magnetic island. In general, the temperature or density profile is flat. However, this flattening is due to a

lack of heat and particle flux inside the magnetic island not due to the enhancement of transport. The transport itself is found to be even smaller inside the magnetic island than that outside the magnetic island, which gives a new insight for understanding the transport and MHD stability when the RMP is applied, because the RMP produced many magnetic islands near the plasma periphery.

Finally, the impact of stochastization on plasma flow and impurity flux have been studied. In LHD plasma, the good impurity shielding due to the stochastic mantic field has been experimentally confirmed. In the low collisional region, the impurity is shielded by the positive radial electric field, while the frictional force outside the LCFS contributes the impurity shielding in the high collisional regime. Therefore, the impurity accumulation takes place only in the narrow parameter space in helical plasma. The understanding in physics of the impurity shield by the stochastic magnetic field can contribute to the prediction of impurity behavior in the plasma with RMP in future devices such as ITER, Wendelstein 7-X[68], FFHR-d1[69], and HELIAS 5-B[70].

The authors would like to thank to the technical staff of the LHD for their support of these experiments.

[1] Kaneko O. *et al* 2013 *Nucl. Fusion* **53** 095024.
[2] Ida K. *et al* 2009 *Nucl. Fusion* **49** 095024.
[3] Nagaoka K. *et al* 2014 *Proceedings of IAEA Fusion Energy Conference* PPC/2-1.
[4] Osakabe M. *et al* 2014 *Plasma Phys. Control. Fusion* **56** 095011.
[5] Takahashi H. *et al* 2013 *Nucl. Fusion* **53** 073034.
[6] Shimozuma T. *et al* 2014 *Proceedings of IAEA Fusion Energy Conference* EX/P6-34.
[7] Fujii, K. Shikama, T. Goto M. *et al* 2013 *Phys. Plasmas* **20** 012514.
[8] Fujii K. *et al* 2014 *Proceedings of IAEA Fusion Energy Conference* EX/P6-31.
[9] Murakami S. *et al* 2014 *Proceedings of IAEA Fusion Energy Conference* TH/P6-38.
[10] Ida K. *et al* 2014 *Nucl. Fusion* **54** 045001.
[11] Yokoyama M. *et al* 2013 *Plasma and Fusion Res.* **8** 2403016.
[12] Yokoyama M. *et al* 2014 *Proceedings of IAEA Fusion Energy Conference* EX/P6-27.
[13] Akiyama T. *et al* 2014 *Proceedings of IAEA Fusion Energy Conference* FIP/P8-31.
[14] Kasahara H. *et al* 2014 *Proceedings of IAEA Fusion Energy Conference* EX/7-3.
[15] Mutoh T. *et al* 2013 *Nucl. Fusion* **53** 063017.
[16] Seki T. *et al* 2014 *Proceedings of IAEA Fusion Energy Conference* FIP/P5-3.
[17] Chowdhuri M.B. *et al* 2009 *Phys. Plasmas* **16** 062502.
[18] Morita S. *et al* 2013 *Nucl. Fusion* **53** 093017.
[19] Ida K. *et al* 2005 *Nucl. Fusion* **45** 391.
[20] Tokitani M. *et al* 2013 *J. Nucl. Mater.* **438** S818.
[21] Shoji M. *et al* 2014 *Proceedings of IAEA Fusion Energy Conference* EX/P6-33.
[22] Ida K., *et al* 2013 *Phys. Rev. Lett.* **111** 055001.
[23] Emoto M. *et al* 2014 *Proceedings of IAEA Fusion Energy Conference* FIP/P8-28.
[24] M. Nunami M., *et al* 2010 *Plasma Fusion Res.* **5** 016.
[25] Nunami M. *et al* 2014 *Proceedings of IAEA Fusion Energy Conference* TH/P7-9.
[26] Nunami M. *et al* 2012 *Phys. Plasmas* **19** 042504.
[27] Rice J., *et al* 2011 *Phys. Rev. Lett.* **107** 265001.
[28] Yoshinuma M. *et al* 2014 *Proceedings of IAEA Fusion Energy Conference* EX / P6-30.
[29] Mikkelsen D.R. *et al* 2014 *Phys. Plasmas* **21** 082302.
[30] Ida K., *et al* 2009 *Phys Plasmas* **16** 056111.
[31] Ida K. *et al.* 2013 *New J. Phys.* **15** 013061.
[32] Inagaki S. *et al* 2013 *Nucl. Fusion* **53** 113006.
[33] Inagaki S. *et al* 2014 *Proceedings of IAEA Fusion Energy Conference* EX/2-1.
[34] Ida K. *et al* 2015 *Nucl. Fusion* **55** 013022.
[35] Inagaki S. *et al* 2011 *Phys. Rev. Lett.* **107** 115001.
[36] Inagaki S. *et al* 2011 *Plasma. Fusion. Res.* **9** 1202052.
[37] Ida K. *et al* 2010 *Nucl. Fusion* **50** 064007.
[38] Takemura Y. *et al* 2012 *Nucl. Fusion* **52** 102001.
[39] Sakakibara S. *et al* 2013 *Nucl. Fusion* **53** 043010.
[40] Sakakibara S. *et al* 2014 *Proceedings of IAEA Fusion Energy Conference* EX/P6-37.
[41] Ishizawa A. *et al* 2014 *Proceedings of IAEA Fusion Energy Conference* TH/P6-40.
[42] Ohdachi S. *et al* 2014 *Proceedings of IAEA Fusion Energy Conference* EX/P6-29.
[43] Narushima Y. *et al* 2014 *Proceedings of IAEA Fusion Energy Conference* EX/P6-35.
[44] Ichiguchi K. *et al* 2014 *Proceedings of IAEA Fusion Energy Conference* TH/6-2.
[45] Tanaka K. *et al* 2013 *Plasma Fusion Res.* **8** 2402141.
[46] Jakubowski M. *et al* 2014 *Proceedings of IAEA Fusion Energy Conference* EX/P3-47.
[47] Evans T. *et al* 2014 *Proceedings of IAEA Fusion Energy Conference* EX/1-3.
[48] Inagaki S. *et al* 2004 *Phys. Rev. Lett.* **92** 055002.
[49] Ida K., *et al* 2012 *Phys. Rev. Lett.* **109** 065001.
[50] Ida K., *et al* 2015 *Nat. Commun.* **6** 5816.
[51] Kamiya K. *et al* 2013 *Nucl. Fusion* **53** 013003.
[52] Du X. *et al* 2014 *Proceedings of IAEA Fusion Energy Conference* EX/P6-36.
[53] Wang H. *et al* 2014 *Proceedings of IAEA Fusion Energy Conference* TH/P1-12.
[54] Osakabe M. *et al* 2014 *Proceedings of IAEA Fusion Energy Conference* EX/10-3.
[55] Kobayashi M. *et al* 2014 *Proceedings of IAEA Fusion Energy Conference* OV/4-4.
[56] S. Masuzaki *et al* 2013 *J. Nucl. Mater* **438** S133.
[57] Kobayashi M. *et al* 2013 *Nucl. Fusion* **53** 093032.
[58] Kobayashi M. *et al* 2010 *Phys. Plasmas* **17** 056111.
[59] Drapiko E.A. *et al* 2011 *Nucl. Fusion* **51** 073005.
[60] Peterson B.J. *et al* 2013 *Plasma Fusion Res.* **8** 2402037.
[61] Mukai K. *et al* 2014 *Proceedings of IAEA Fusion Energy Conference* EX/P6-25.
[62] Ohno N. *et al* 2014 *Proceedings of IAEA Fusion Energy Conference* EX/P6-26.
[63] Kawamura G. *et al* 2014 *Proceedings of IAEA Fusion En-*

ergy Conference TH/P6-39.
[64] Sudo S. *et al* 2014 *Proceedings of IAEA Fusion Energy Conference* EX/P6-32.
[65] Ohyabu N. *et al* 2006 *Phys. Rev. Lett.* **97** 055002.
[66] Sudo S. *et al* 2013 *Plasma Phys. Contol. Fusion* **55** 095014.
[67] Murakami I. *et al* 2014 *Proceedings of IAEA Fusion Energy Conference* EX/P6-28.
[68] Dinklage A. *et al* 2014 *Proceedings of IAEA Fusion Energy Conference* FIP/3-1.
[69] Goto T. *et al* 2014 *Proceedings of IAEA Fusion Energy Conference* FIP/P7-16.
[70] Schauer, F. Egorov K. and Bykov V. 2013 *Fusion Engineering and Design* **88** 1619.

Collaborators*

J.W. Ahn[1] E. Ascasibar[2] J. Baldzuhn[3] D. López-Bruna[2] F. Castejón[2] M.B. Chowdhuri[4] W. Gao[5] D. Gradic[3] J.M. Garcia-Regana[3] L. Heinrich[3] W. Horton[6] W.H. Ko[7] J.H. Lee[7] A. Melnikov[8] M. O'Mullane[9] J.K. Park[10] M. Preynas[3] C. Skinner[10] I. Sharov[10] O. Schmitz[11] T. Stange[3] J.L. Velasco[2] E. Winkler[3] M. Zarnstorff[10] G. Yun[12] D. Nishijima[13] N. Ezumi[14] Y. Hayashi[17] T. Higashiguchi[15] M. Itagaki[16] A. Kohyama[17] F. Koike[18] S. Kobayashi[14] K. Koga[19] O. Mitarai[20] H. Matsuura[21] Y. Matsumoto[22] R. Makino[23] M. Nishiura[24] Y. Nobuta[25] Y. Nakamura[26] M. Okamoto[27] R. Soga[23] K. Sawada[28] M. Shiratani[29] Y. Takeuchi[30] N. Tsujii[31] Y. Tanaka[32] T. Watanabe[33] N. Yoshida[34] N. Yamaguchi[35] Y. Yamauchi[36] E. Yatsuka[37]

[1]Oak Ridge National Laboratory, Oak Ridge, TN 37831, USA
[2]Laboratorio Nacional de Fusion, Asociacion EURATOM-CIEMAT, 28040 Madrid, Spain
[3]Max-Planck-Institut für Plasmaphysik, Wendelsteinstr. 1, 17489 Greifswald, Germany
[4]Institute for Plasma Research, Bhat, Gandhinagar 382 428, India
[5]Institute of Plasma Physics, PO Box 1126, Hefei, Anhui 230031, Peoples Republic of China
[6]Institute for Fusion Studies, University of Texas at Austin, Austin, TX 78712, USA
[7]National Fusion Research Institute, Daejeon, Korea
[8]Russian Research Centre Kurchatov Institute, Institute of Nuclear Fusion,1, Kurchatov Sq., Moscow, 123182 Russia
[9]Department of Physics, University of Strathclyde,107 Rottenrow, Glasgow, G4 0NG, United Kingdom
[10]St. Petersburg State PolyTechnical University, 29 Politechnicheskaya, St.Petersburg 195251,Russia
[11]Department of Engineering Physics University of Wisconsin - Madison 1500 Engineering Drive Madison, WI 53706, USA
[12]POSTECH, Pohang, Gyeongbuk 790-784, Republic of Korea
[13]Center for Energy Research, University of California, San Diego, U.S.A.
[14]Nagano National College of Technology, 716 Tokuma, Nagano 381-8550, Japan
[15]Department of Advanced Interdisciplinary Sciences, Center for Optical Research and Education (CORE), Utsunomiya University, 7-1-2 Yoto, Utsunomiya 321-8585, Japan
[16]Division of Quantum Science and Engineering, Faculty of Engineering, Hokkaido University Kita-13, Nishi-8, Kita-ku, Sapporo, 060-8628 Japan
[17]Department of material science and metallurgy, Organization of Advanced Sustainability Initiative for Energy System/Materials, Muroran Institute of Technology
[18]Faculty of Science and Engineering, Sophia University, 7-1 Kioi-cho, Chiyoda-ku Tokyo 102-8554 Japan
[19]Department of Electronics, Kyushu University, 744 Motooka, Fukuoka 819-0395, Japan
[20]Institute of Industrial Science and Technical Research, Tokai University, 9-1-1 Toroku, Kumamoto 862-8652, Japan
[21]Radiation Research Center, Osaka Prefecture University, 1-2 Gakuen-cho, Sakai Naka-ku, 599-8570 Osaka, Japan
[22]Faculty of Engineering, Hokkaido University Kita, 13, Nish 8 Kita-ku, Sapporo 060-8628, Japan
[23]Department of Energy Engineering and Science, Nagoya University, Furo-cho, Chikusa, Nagoya 464-8603, Japan
[24]Department of Advanced Energy, Division of Transdisciplinary Sciences, Graduate School of Frontier Sciences The University of Tokyo, 5-1-5 Kashiwanoha, Kashiwa, Chiba 277-8561 Japan
[25]Division of Quantum Science and Engineering,Faculty of Engineering, Hokkaido University N13 W8, Kita-ku, Sapporo 060-8628, Japan
[26]Graduate School of Energy Science, Kyoto University, Gokasho, Uji, Kyoto 611-0011, Japan
[27]Ishikawa National College of Technology, Kitacyujo, Tsubata, Ishikawa, 929-0392, Japan
[28]Department of Applied Physics, Faculty of Engineering, Shinshu University, 4-17-1 Wakasato, Nagano 380-8553, Japan
[29]Graduate School of Information Science and Electrical Engineering, Kyushu University 744 Motookai, Nishi-ku, Fukuoka, 819-0395,Japan
[30]Department of Information Systems, Daido University 10-3 Takiharu-cho, Minami-ku, Nagoya, 457-8530, Japan
[31]Graduate School of Frontier Sciences, The University of Tokyo, Kiban-tou, 5-1-5 Kashiwanoha, Kashiwa, Chiba 277-8561, Japan
[32] Division of Electrical Engineering and Computer Science, Kanazawa University, Kakuma, Kanazawa 920-1192, Japan
[33] National Astronomical Observatory of Japan, 2-21-1 Osawa, Mitaka, Tokyo?181-8588, Japan
[34]Research Institute for Applied Mechanics, Kyushu University, 6-1 Kasuga-kouen, Kasuga, Fukuoka 816-8580, Japan

[35] Physics Laboratory, Graduate School of Medicine and Pharmaceutical Sciences, University of Toyama, Toyama 930-0194, Japan
[36] Division of Quantum Science and Engineering,Faculty of Engineering, Hokkaido University N13 W8, Kita-ku, Sapporo 060-8628, Japan
[37]Japan Atomic Energy Agency, Naka, Ibaraki-ken, 311-0193, Japan